ACS APPLIED MATERIALS & INTERFACES

Research Article

www.acsami.org

Ag/BiOBr Film in a Rotating-Disk Reactor Containing Long-Afterglow Phosphor for Round-the-Clock Photocatalysis

Haibo Yin, Xiaofang Chen, Rujing Hou, Huijuan Zhu, Shiqing Li, Yuning Huo,* and Hexing Li*

The Education Ministry Key Lab of Resource Chemistry, Shanghai Key Laboratory of Rare Earth Functional Materials, Shanghai Normal University, Shanghai 200234, China

Supporting Information

ABSTRACT: Ag/BiOBr film coated on the glass substrate was synthesized by a solvothermal method and a subsequent photoreduction process. Such a Ag/BiOBr film was then adhered to a hollow rotating disk filled with long-afterglow phosphor inside the chamber. The Ag/BiOBr film exhibited high photocatalytic activity for organic pollutant degradation owing to the improved visible-light harvesting and the separation of photoinduced charges. The long-afterglow phosphor could absorb the excessive daylight and emit light around 488 nm, activating the Ag/BiOBr film to realize round-the-clock photocatalysis. Because the Ag nanoparticles could extend the light absorbance of the Ag/BiOBr film to wavelengths of around 500 nm via a surface plasma resonance effect, they played a key role in realizing photocatalysis induced by long-afterglow phosphor.

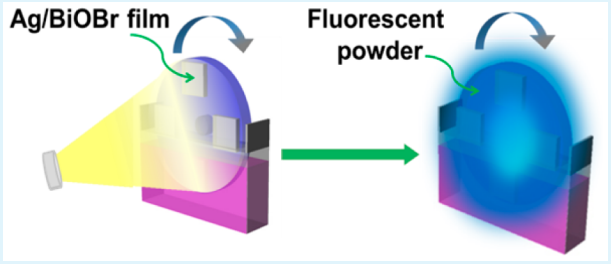

KEYWORDS: *Ag/BiOBr film, rotating-disk reactor, visible-light photocatalyst, long-afterglow phosphor, round-the-clock photocatalysis*

INTRODUCTION

Photocatalysis shows good potential in environmental cleaning by mineralizing organic pollutants.[1,2] Most studies are focused on the design of visible-light photocatalysts with the aim of making efficient use of sunlight. The BiOBr visible photocatalyst has attracted increasing attention for its high activity and strong stability.[3−5] Meanwhile, a Ag-modified semiconductor has also been widely studied owing to the dual functions of Ag nanoparticles for both inducing visible-light photocatalysis by a surface plasma resonance (SPR) effect and promoting photoelectron−hole separation.[6−8] In addition, a photocatalysis reactor is also essential to enhancing the photocatalytic efficiency.[9,10] Various reactors have been developed such as the annular photoreactor,[11,12] photocatalytic Taylor vortex reactor,[13] fluidized-bed reactor,[14] and corrugated-plate reactor.[15,16] However, photocatalysis still displays some instinct problems. One is its poor light-harvesting ability owing to the light-shielding effect by the solution, especially by the colorful solution containing dye pollutants. The other is that photocatalysis cannot proceed at night because of the absence of light irradiation. This is significant to realizing a round-the-clock photocatalytic process via the transformation of redundant energy during light irradiation to the mediate that could continuously provide light at night.

Herein, we developed a novel photocatalysis reactor containing a hollow rotating glass disk coated with a Ag/BiOBr film on the outer surface and filled with long-afterglow phosphor inside the chamber (see Scheme 1). The Ag/BiOBr film acted as a visible-light photocatalyst, while the rotating disk could avoid the light-shielding effect by the solution. More importantly, the long-afterglow phosphor could absorb and store excessive sunlight in the daytime, followed by emitting light with a characteristic wavelength of around 488 nm at night to drive round-the-clock photocatalysis. Taking into account that BiOBr could be activated only by visible light with wavelength of around 420 nm, the Ag nanoparticles having a SPR effect of around 500 nm could start photocatalysis at night by absorbing the emission light from long-afterglow phosphor. The Ag nanoparticles located on BiOBr could also promote photocatalysis by enhancing light harvesting and inhibiting photoelectron−hole recombination. Additionally, the rotating-disk reactor with the Ag/BiOBr film could solve the problem of separation and recovery of the powder catalyst in practical applications.

Scheme 1. Schematic of a Rotating-Disk Reactor with Long-Afterglow Phosphor

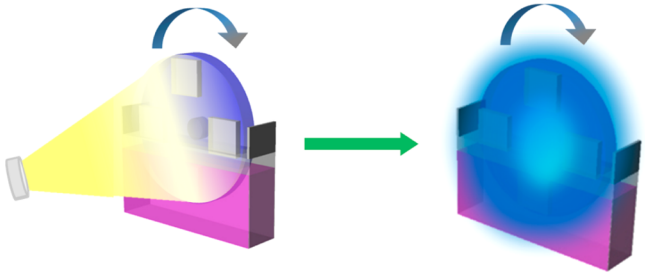

Received: June 11, 2015
Accepted: August 28, 2015
Published: August 28, 2015

DOI: 10.1021/acsami.5b05184
ACS Appl. Mater. Interfaces 2015, 7, 20076−20082

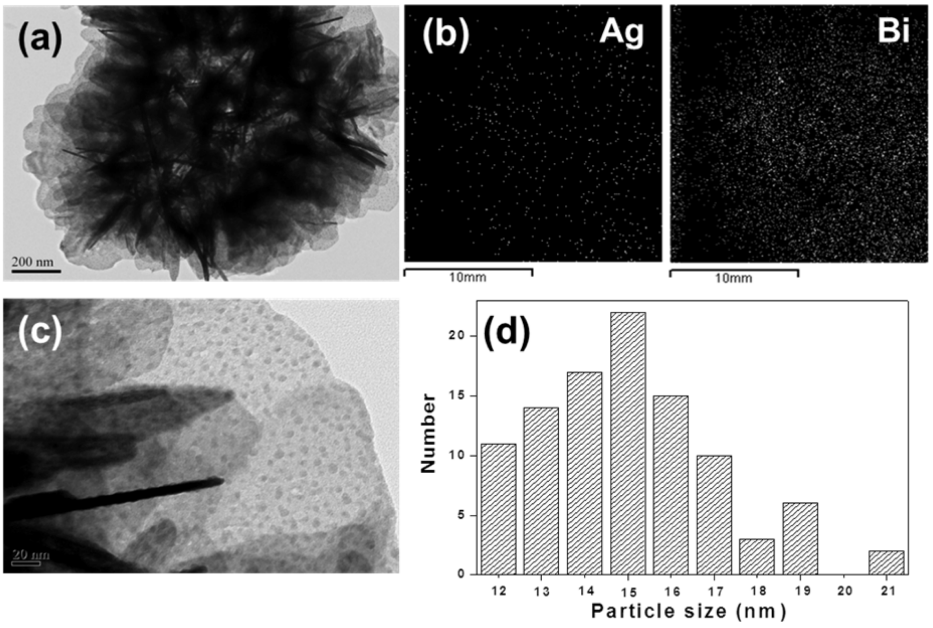

Figure 1. (a) TEM image. (b) Chemical mapping of Ag and Bi elements. (c) High-resolution TEM image. (d) Ag particle size distribution of the Ag/BiOBr-3.0-15 sample.

EXPERIMENTAL SECTION

Photocatalyst Preparation. The BiOBr film was synthesized according to our previous work as the following process. After pretreatment of the soda glass sheet (2.5 × 2.2 cm^2), 0.12 g of $Bi(NO_3)_3{\cdot}5H_2O$ was dissolved in a mixture solution with 5.0 mL of ethylene glycol and 35 mL of isopropyl alcohol. Then, $[C_{16}mim]BrIL$ was also dissolved with a Bi/Br molar ratio of 1:2 and stirred vigorously for 1.5 h. Then, one glass plate was put inside a 50 mL Teflon-lined stainless steel autoclave, and the obtained solution was then transferred into it. After that, the autoclave was sealed and maintained at 160 °C for 8 h, followed by natural cooling to room temperature. The obtained films were cleaned three times with ethanol and deionized water and dried at ambient temperature for 1.0 h. Finally, the films were calcined at 400 °C for 4 h to improve crystallization of the catalyst and remove the organic residuals.

A photoreduction approach was used to deposit Ag nanoparticles on BiOBr films. Three as-prepared BiOBr films were placed in a 60 mL methyl alcohol solution dissolved with $AgNO_3$ with the desired Ag/Bi molar ratio. Then, the solution was irradiated under one ultraviolet light (365 nm, 8 W) with different times. Finally, the films were washed three times with ethanol and water. The samples were denoted as Ag/BiOBr-*X*-*Y*, in which *X* and *Y* represented the Ag/Bi molar ratio (%) and photoreduction time (min), respectively.

Finally, four glass sheets (each size = 2.5 × 2.2 cm) coated with the Ag/BiOBr film were uniformly adhered onto the outer surface of a rotating disk (7.9 cm diameter and 1.2 cm thickness) filled with 74.4 g of long-afterglow phosphor (Blue NL-PA, Shanghai Congyu Company; characteristic wavelength of around 488 nm) inside the chamber.

Characterization. The structure was detected by X-ray diffraction (XRD; Rigacu D/Max-2000). Surface morphologies were observed by field-emission scanning electron microscopy (FESEM; Hitachi S-4800) and transmission electron microscopy (TEM; JEM-2010). X-ray photoelectron spectroscopy (XPS; Versa Probe PHI 5000) was used to determine surface electronic states. The shift of the binding energy due to relative surface charging was corrected using the C1S level at 284.8 eV as an internal standard. The optical property was analyzed by both UV−vis diffuse-reflectance spectroscopy (DRS; MC-2530) and photoluminescence (PL) spectroscopy (Varian Cary-Eclipse 500). The measurement system of surface photovoltage spectroscopy (SPS) was assembled by a source of monochromatic light, a light chopper (SR540, Stanford), and a lock-in amplifier (SR830-DSP, Stanford). A 500 W Xe lamp (CHF XM500W, Stusttech) and a double-prism monochromator (Omini-500, Zolix) were combined to provide monochromatic light with a chopping frequency of 23 Hz. Time-resolved fluorescence spectra were measured on a Horiba Scientific Fluoro-Cube based on the principle of time-correlated single-photon counting.

Activity Test. Photodegradation of rhodamine B (RhB) was conducted in the reactor illustrated in Scheme 1 at 30 °C. The rotating disk was immersed into 55 mL of a 10 mg/L RhB solution with 57% of the disk surface exposed to air. The disk was rotated for 30 min in the dark at a speed of 90 rpm to achieve adsorption−desorption equilibrium. Then, photocatalysis was initiated by illumination with a 300 W Xe lamp (CHF-XM500; light intensity = 600 mW/cm^2) located 10 cm away. All of the UV light with wavelength of less than 420 or 450 nm was removed by the glass filters. The reaction continued in the dark by Blue NL-PA long-afterglow phosphor (λ = 488 nm) after the Xe lamp was turned off. At given time intervals, the initial concentration of RhB (C) was measured on a UV−vis spectrophotometer (UV-7502PC, XinMao Instrument Co. Ltd., Shanghai) at the characteristic wavelength of 553 nm. Preliminary tests demonstrated a good linear relationship between the light absorbance and RhB concentration. The degradation yield was calculated by comparing the RhB concentration during the reaction (C) with the initial concentration (C_0). The reproducibility of the results was checked by repeating the experiments at least three times and was found to be within acceptable limits (±5%). The apparent quantum efficiency for chemical species is often defined as the initial measured rate of photodegradation divided by the theoretical maximum rate of photon absorption, which is expressed as follows:[17−19]

$$\varphi_x = \frac{\pm \mathrm{d}[x]/\mathrm{d}t}{\mathrm{d}[h\nu]_{\mathrm{inc}}/\mathrm{d}t}$$

where $\mathrm{d}[x]/\mathrm{d}t$ is either the initial rate of formation or loss of chemical species and $\mathrm{d}[h\nu]_{\mathrm{inc}}/\mathrm{d}t$ is the total optical power impinging on the sample. According to the above equation, the optical power and apparent quantum efficiency for different reaction processes was determined as follows:

$$\text{initial optical power } \Phi_{\text{visible light}} = \int_{\lambda_0}^{\lambda_1} \frac{W_0 \lambda}{hc}\, \mathrm{d}\lambda$$

DOI: 10.1021/acsami.5b05184
ACS Appl. Mater. Interfaces 2015, 7, 20076−20082

optical power on a rotating disk $\Phi_{\text{rotating disk}}$

$$= \left(\int_{\lambda_0}^{\lambda_1} \frac{W_0 \lambda}{hc} \, d\lambda \right) (57\% + 43\% \times 10\%)$$

optical power of long-afterglow phosphor $\Phi_{\text{long-afterglow phosphor}}$

$$= \frac{W_1 \lambda_2}{hc} (57\% + 43\% \times 10\%)$$

apparent quantum efficiency $\varphi = N/\Phi$

where W_0 = 300 W, $h = 6.626 \times 10^{-34}$, $c = 3.0 \times 10^8$ m/s, λ_0 = 420 nm, λ_1 = 780 nm, W_2 = 20 mW, λ_2 = 488 nm, and N = number of reacted organic molecules. The rotating disk was immersed in a RhB solution with 57% of the disk surface exposed to air, and only about 10% of the light could reach the catalyst film with a rotating disk of 1.2 cm thickness.

The durability of the catalyst films coated on the rotating disk with long-afterglow phosphor was measured according to the following procedure. After each run of the photocatalysis reactions, the films were washed with distilled water three times and dried at 100 °C for 12 h. Then, each recycling test was conducted under the same conditions, and the RhB photodegradation rate was determined to show the change of activity.

Adsorption Test. The adsorption ability of different samples was investigated via the uniform localization of four glass sheets (each size = 2.5 × 2.2 cm) coated with catalyst films on the rotating disk reactor in the dark with a rotating speed of 90 rpm. It was immersed in 55 mL of a 10 mg/L aqueous RhB solution at 30 °C. A total of 57% of the surface area of the disk was exposed to air. At given time intervals, the initial concentration of organics (C_0) and concentration during the adsorption process (C) were measured to calculate the adsorption rate.

RESULTS AND DISCUSSION

Structure Characteristics. FESEM images (Figure S1) show that the Ag/BiOBr nanosheets uniformly grew on the glass substrate. No Ag particles are observed owing to the high dispersion and small size. The TEM and chemical mapping images together with the Ag particle size distribution pattern in Figure 1 clearly display the uniform Ag nanoparticles on BiOBr nanosheets with an average size of around 15 nm.

As shown in Figure 2, the XRD patterns demonstrate that both BiOBr and Ag/BiOBr-3.0-15 films exhibit a pure tetragonal BiOBr crystal phase (JCPDS 09-0393). No significant peaks indicative of Ag are found because of the high dispersion of small Ag nanoparticles with very low loading. The XPS spectra (Figure S2) demonstrate that all Ag species were present in the metallic state, corresponding to binding energies of around 367.7 and 373.7 eV in $Ag_{3d5/2}$ and $Ag_{3d3/2}$, respectively, with a difference of 6.0 eV.[20−22] According to XPS and inductively coupled plasma (ICP) analysis, the concentrations of Ag nanoparticles in different samples are summarized in Table 1. XPS and ICP analysis demonstrated that the Ag loading increased with an increase in either the initial $AgNO_3$ concentration or the photoreduction period and reached a saturated value. The actual concentration of Ag nanoparticles from the XPS results was much higher than that from the ICP results, obviously because of the main deposition of Ag nanoparticles on the surface of the BiOBr film.

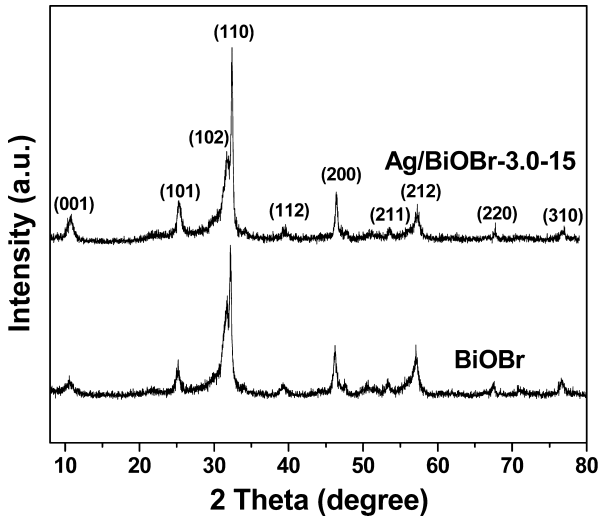

Figure 2. XRD patterns of different samples.

Table 1. Concentration of Ag in Different Samples

sample	Ag/Bi (theoretical value) (mol %)	Ag/Bi (XPS result) (mol %)	Ag/Bi (ICP result) (mol %)
BiOBr	0	0	0
Ag/BiOBr-1.5-15	1.5	0.11	0.030
Ag/BiOBr-3.0-15	3.0	0.45	0.11
Ag/BiOBr-4.5-15	4.5	0.95	0.13
Ag/BiOBr-6.0-15	6.0	0.97	0.13
Ag/BiOBr-3.0-10	3.0	0.34	0.050
Ag/BiOBr-3.0-20	3.0	0.87	0.14
Ag/BiOBr-3.0-25	3.0	1.1	0.15

Optical Properties. From UV−vis DRS spectra in Figure 3, the Ag/BiOBr-3.0-15 film presents stronger visible-light absorption from 400 to 600 nm than the pure BiOBr film owing to the Ag SPR.[23,24] The excessive Ag nanoparticles in the Ag/BiOBr-6.0-15 film result in the small SPR. Additionally, Ag/BiOBr-3.0-15 also shows stronger SPS response than BiOBr, indicating the higher separation efficiency of photoinduced charge carriers and the stronger surface charge transfer under light irradiation,[25] which is consistent with the PL spectra in Figure S3. Ag/BiOBr-3.0-15 shows the lowest PL peak intensity among all of the films. In comparison, the smaller Ag−BiOBr interface in Ag/BiOBr-1.5-15 is not beneficial for charge separation, and an excessive Ag amount in both Ag/BiOBr-4.5-15 and Ag/BiOBr-6.0-15 could lead to easy charge recombination on Ag nanoparticles.[25−27] The increased PL decay time of Ag/BiOBr-3.0-15 over that of BiOBr (Figure S4) was also attributed to the reduced recombination of the electrons and holes on the Ag/BiOBr film surface,[27] owing to the electron-trapping effect of Ag nanoparticles. Meanwhile, long-afterglow phosphor (Blue NL-PA) emitted visible light around 488 nm (Figure S5) at an excitation light of 400 nm, which could activate the Ag/BiOBr photocatalyst.

Photocatalytic Performance. According to the similar RhB adsorption rate and capability on the Ag/BiOBr-3.0-15 and BiOBr films (Figure S6), the influence of the RhB adsorption property on different catalyst films could be excluded during the photocatalytic degradation process. First, we examined the role of the rotating disk by using the BiOBr film photocatalyst to exclude the influence from Ag nanoparticles. Both a color solution containing RhB and a colorless

DOI: 10.1021/acsami.5b05184
ACS Appl. Mater. Interfaces 2015, 7, 20076−20082

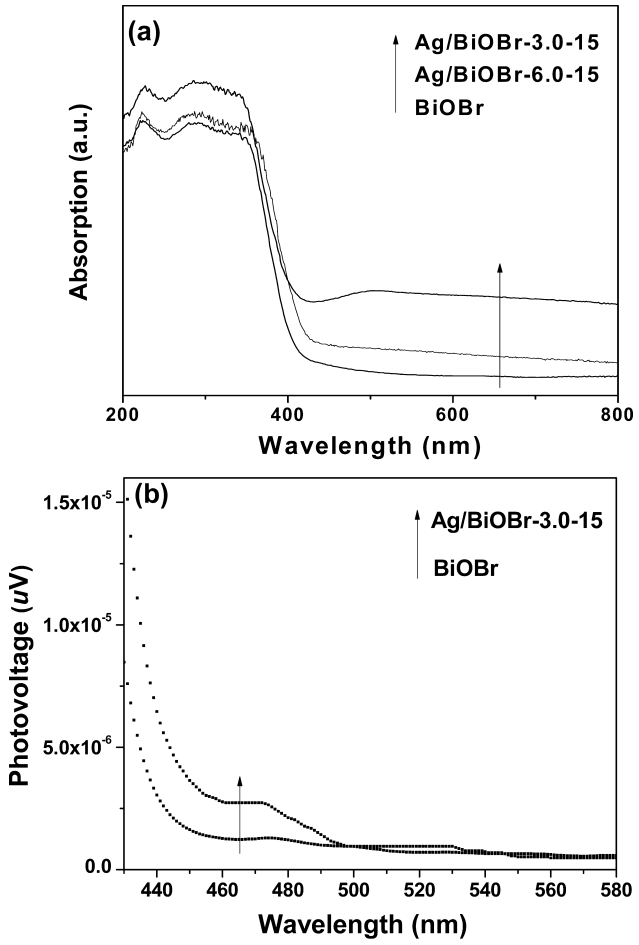

Figure 3. (a) UV–vis DRS and (b) SPS spectra of different films.

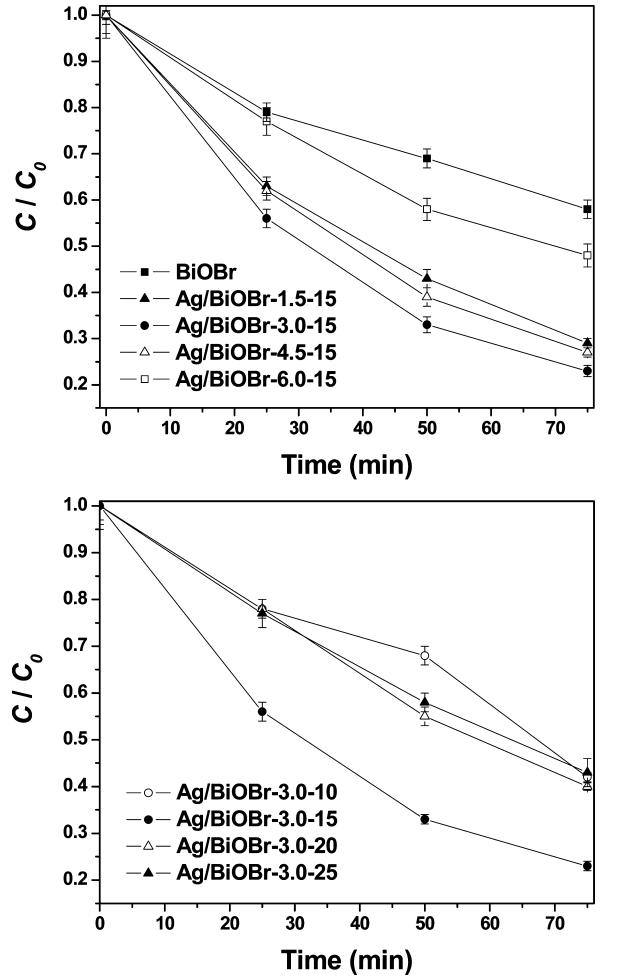

Figure 4. Photodegradation of RhB on (a) Ag/BiOBr-X-15 and (b) Ag/BiOBr-3.0-Y films in the rotating-disk reactor without long-afterglow phosphor. Reaction conditions: four glass plates (each size = 2.5 × 2.2 cm) coated with catalysts localized on the disk; 55 mL of a 10 mg/L RhB aqueous solution; reaction temperature = 30 °C; one 300 W Xe lamp (light intensity = 600 mW/cm^2; λ > 420 nm); rotating speed = 90 rpm.

solution containing 2,4-dichlorophenol were used (see Figures S7 and S8). The BiOBr film on the rotating disk with a speed of 90 rpm exhibited much higher activity than either the BiOBr powder scrapped from the BiOBr film immersed in the solution or the BiOBr film on the static rotating disk. We also found that the promoting effect of the rotating disk became more significant by using a color solution containing RhB than that by using a colorless solution containing 2,4-dichlorophenol. As is known, a color solution could absorb more light, leading to an enhanced light-shielding effect, especially at high RhB concentration. Our preliminary test demonstrated that only about 30% and 10% of the light could reach the photocatalyst at a depth of 1 cm in a colorless solution containing 10 mg/L 2,4-dichlorophenol and in a color solution containing 10 mg/L RhB, respectively. When the disk was rotated, only less than a 1 mm solution film was coated on the disk. Thus, light could easily pass through such a thin solution film to reach the photocatalyst with little light loss even in the presence of 10 mg/L RhB, which could ensure high photocatalytic degradation efficiencies. Furthermore, the BiOBr film coated on the rotating disk presented a higher apparent quantum efficiency than that coated on the static disk and BiOBr powder dispersed in solution during the photocatalytic degradation of both RhB and 2,4-dichlorophenol, as shown in Table S1.

Second, the photocatalytic activity of the Ag/BiOBr film on the rotating disk without long-afterglow phosphor was investigated. As shown in Figure 4, Ag/BiOBr films with increasing Ag loading obtained by enhancing either the initial $AgNO_3$ concentration or photoreduction time display first an increase and then a decrease in the photocatalytic activity. The Ag/BiOBr-3.0-15 film exhibits the highest photocatalytic activity under visible-light irradiation. This could be mainly ascribed to the enhanced visible-light harvest due to the SPR of Ag nanoparticles and the diminished photoinduced electron–hole recombination rate due to rapid photoinduced electron transfer through the Ag nanopartcles.[27] The excessive Ag loading is harmful for photocatalysis because of the gathering of Ag nanoparticles, which diminishes the SPR effect and the inhibiting effect on the charge recombination. In order to further investigate the effect of Ag particles, Figure S9 presents the photocatalytic process in the rotating-disk reactor without long-afterglow phosphor under different visible-light irradiation. Both the effect of the SPR and charge separation of the Ag nanoparticles result in the greatly enhanced activity of the Ag/BiOBr-3.0-15 film at λ > 420 nm over that of other conditions. In comparison, the slightly improved activity of Ag/BiOBr-3.0-15 over that of the BiOBr film at λ > 450 nm is only due to photoinduced electron–hole separation via electron trapping by Ag nanoparticles.[28,29] Meanwhile, under light irradiation

DOI: 10.1021/acsami.5b05184
ACS Appl. Mater. Interfaces 2015, 7, 20076–20082

with λ > 450 nm, hot electrons could reach the interface between the metal Ag and BiOBr catalyst, overcome the potential barrier at the interface, and then be transported into BiOBr, beneficial for improvement of the photodegradation activity.[30−32]

Figure 5 shows the photocatalytic degradation process of RhB on the BiOBr or Ag/BiOBr-3.0-15 film coated on the rotating disk filled with or without long-afterglow phosphor. Under visible-light irradiation, the BiOBr film in the presence of long-afterglow phosphor exhibited slightly higher activity than that without long-afterglow phosphor. This could be attributed to the fact that the visible light with a wavelength of around 488 nm emitted from long-afterglow phosphor could not efficiently activate the BiOBr film, which absorbed light around 420 nm. This could also account for the fact that, after the Xe light was turned off, only a trace RhB could be continuously degraded under irradiation with light emitted from long-afterglow phosphor. Interestingly, the Ag/BiOBr-3.0-15 film exhibited much higher photocatalytic activity in the presence of long-afterglow phosphor filled in the rotating disk than that in the absence of long-afterglow phosphor. This could be attributed to the unique SPR effect of Ag nanoparticles, corresponding to the absorbing light with a wavelength of up to 500 nm. As a result, the Ag/BiOBr film could be activated by light emitted from long-afterglow phosphor (~488 nm). This also ensured continuous photocatalytic degradation of RhB after the Xe light was turned off, leading to round-the-clock photocatalysis. Long-afterglow phosphor first adsorbed visible light from the Xe light. After the Xe light was turned off, light was emitted around 488 nm, which could also activate Ag/BiOBr for subsequent photocatalysis owing to the SPR effect of the Ag nanoparticles. The Ag nanoparticles could be oxidized by the plasma-induced charges and simultaneously reduced by the electrons from the BiOBr conduction band.[33] This could be confirmed by XPS spectra in Figure S10, which display no significant change of metallic Ag after different light irradiation. Meanwhile, it could be found in Table S2 that the Ag/BiOBr-3.0-15 film in the rotating-disk reactor filled with long-afterglow phosphor presented the highest apparent quantum efficiency in comparison to other reaction systems. Additionally, the optimal rotation rate in the rotating-disk reactor filled with long-afterglow phosphor was determined to be 90 rpm during the photocatalytic degradation process (Figure S11). This could possibly be attributed to the fact that the low rotation rate was not beneficial for reactant adsorption and the high rotation rate is harmful for light utilization.

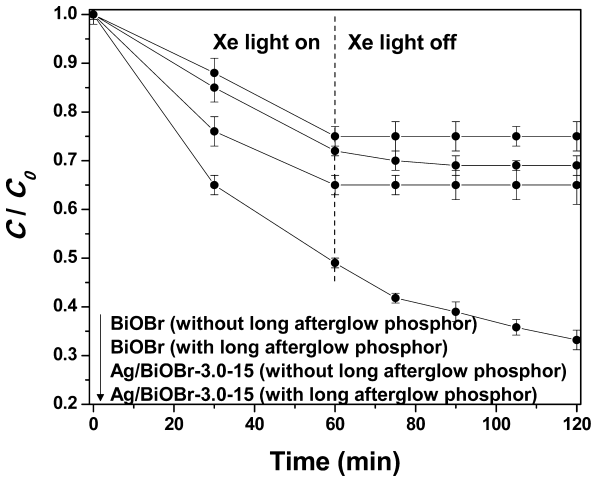

Figure 5. Photodegradation of RhB on different films in the rotating-disk reactor filled with or without long-afterglow phosphor. Reaction conditions: four glass plates (each size = 2.5 × 2.2 cm) coated with catalysts localized on the disk; 55 mL of 15 mg/L RhB aqueous solution; reaction temperature = 30 °C; one 300 W Xe lamp (light intensity = 600 mW/cm^2; λ > 420 nm); Blue NL-PA long-afterglow phosphor (λ = 488 nm); rotating speed = 90 rpm.

The Ag/BiOBr-3.0-15 and BiOBr films in different reaction processes present no significant decrease of the photoactivity after recycling six times, as shown in Figure 6. Furthermore, little significant light absorption change of both the Ag/BiOBr-3.0-15 and BiOBr films after recycling six times could be found in the UV−vis spectra (Figure S12). The high durability implied stable interaction of the Ag nanoparticles with the BiOBr film and structure stability of the BiOBr film, suitable for repetitive utilization in practical applications, against either structural damage or leaching from the glass substrate.

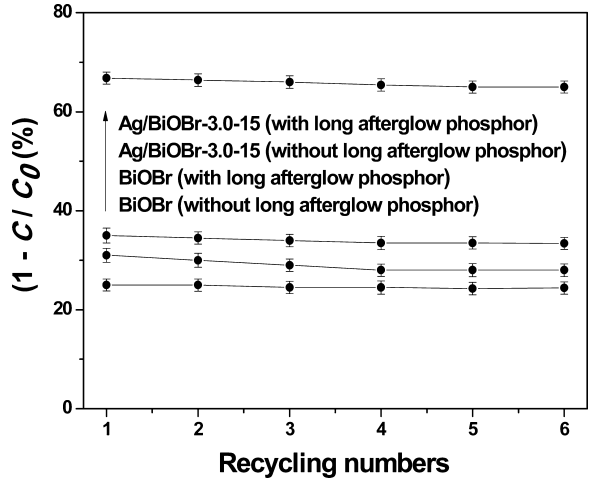

Figure 6. Recycling test of different films in the rotating-disk reactor filled with or without long-afterglow phosphor. Reaction conditions are given in Figure 5.

CONCLUSION

This work developed an Ag/BiOBr composite photocatalysis system for degradation of organic pollutants in wastewater. The Ag/BiOBr film was coated on the outer surface of a rotating-disk reactor filled with long-afterglow phosphor. It exhibited high photocatalytic activity owing to the improved visible-light harvesting and lower recombination efficiency of the photo-induced charges. The light-shielding effect of the color solution containing dye pollutants could be easily avoided by rotation of the disk. More importantly, long-afterglow phosphor could store excessive irradiation light and then emit light around 488 nm in the absence of light irradiation, which activated the Ag/BiOBr film for continuous photocatalysis, leading to round-the-clock photocatalysis. The Ag nanoparticles extended the light absorbance of the Ag/BiOBr film to around 500 nm via the SPR effect. Thus, the Ag/BiOBr film could be activated by light emitted from long-afterglow phosphor. This photocatalytic system also exhibited strong durability and could be used repetitively, showing good potential in the practical cleaning of dyeing wastewater.

DOI: 10.1021/acsami.5b05184
ACS Appl. Mater. Interfaces 2015, 7, 20076−20082

■ ASSOCIATED CONTENT

Supporting Information

The Supporting Information is available free of charge on the ACS Publications website at DOI: 10.1021/acsami.5b05184.

Apparent quantum efficiencies in different reaction systems, FESEM images of BiOBr and Ag/BiOBr-3.0-15 films, XPS spectra of Ag in different samples, PL spectra of different films excited by 400 nm light, PL decay curves of different films that were excited at 455 nm and monitored at 530 nm, PL spectrum of long-afterglow phosphor excited by 400 nm light, RhB adsorption on the BiOBr and Ag/BiOBr-3.0-15 films coated on a rotating disk, reaction profiles of RhB photocatalytic degradation on a BiOBr powder by scraping the BiOBr film from the glass substrate and the BiOBr film coated on the rotating or static disk without long-afterglow phosphor, reaction profiles of 2,4-dichlorophenol photocatalytic degradation on a BiOBr powder by scraping the BiOBr film from the glass substrate and the BiOBr film coated on the rotating or static disk without long-afterglow phosphor, photodegradation of RhB on different films in the rotating-disk reactor without long-afterglow phosphor under different visible-light irradiation, XPS spectra of Ag in the Ag/BiOBr-3.0-15 film, RhB photodegradation on the Ag/BiOBr-3.0-15 film in the rotating-disk reactor filled with long-afterglow phosphor at different rotating speeds, and UV−vis DRS spectra of the Ag/BiOBr-3.0-15 and BiOBr films before and after recycling tests in the rotating-disk reactor filled with long-afterglow phosphor (PDF)

■ AUTHOR INFORMATION

Corresponding Authors

*E-mail: Huoyuning@shnu.edu.cn. Phone: +86-21-64322642. Fax: 86-21-6432-2272.

*E-mail: Hexing-li@shnu.edu.cn. Phone: +86-21-64322642. Fax: 86-21-6432-2272.

Author Contributions

The manuscript was written through contributions of all authors. All authors have given approval to the final version of the manuscript.

Notes

The authors declare no competing financial interest.

■ ACKNOWLEDGMENTS

This work was supported by the National Natural Science Foundation of China (Grants 21261140333, 21237003, 21207091, and 21577092), the Program for Changjiang Scholars and Innovative Research Team in University (IRT1269), and the International Joint Laboratory on Resource Chemistry.

■ REFERENCES

(1) Kubacka, A.; Fernández-García, M.; Colón, G. Advanced Nanoarchitectures for Solar Photocatalytic Applications. *Chem. Rev.* **2012**, *112*, 1555−1614.

(2) Jiang, Z.; Yang, F.; Yang, G. D.; Kong, L.; Jones, M. O.; Xiao, T. C.; Edwards, P. P. The Hydrothermal Synthesis of BiOBr Flakes for Visible-Light-Responsive Photocatalytic Degradation of Methyl Orange. *J. Photochem. Photobiol., A* **2010**, *212*, 8−13.

(3) Ai, Z. H.; Ho, W.; Lee, S.; Zhang, L. Z. Efficient Photocatalytic Removal of NO in Indoor Air with Hierarchical Bismuth Oxybromide Nanoplate Microspheres under Visible Light. *Environ. Sci. Technol.* **2009**, *43*, 4143−4150.

(4) Huo, Y. N.; Zhang, J.; Miao, M.; Jin, Y. Solvothermal Synthesis of Flower-Like BiOBr Microspheres with Highly Visible-Light Photocatalytic Performances. *Appl. Catal., B* **2012**, *111−112*, 334−341.

(5) Zhang, L.; Cao, X. F.; Chen, X. T.; Xue, Z. L. BiOBr Hierarchical Microspheres: Microwave-Assisted Solvothermal Synthesis, Strong Adsorption and Excellent Photocatalytic Properties. *J. Colloid Interface Sci.* **2011**, *354*, 630−636.

(6) Cui, Y. F.; Briscoe, J.; Dunn, S. Effect of Ferroelectricity on Solar-Light-Driven Photocatalytic Activity of $BaTiO_3$: Influence on the Carrier Separation and Stern Layer Formation. *Chem. Mater.* **2013**, *25*, 4215−4223.

(7) Han, L.; Xu, Z. K.; Wang, P.; Dong, S. J. Facile Synthesis of A Free-Standing Ag@AgCl Film for A High Performance Photocatalyst and Photodetector. *Chem. Commun.* **2013**, *49*, 4953−4955.

(8) Zhang, L. S.; Wong, K. H.; Yip, H. Y.; Hu, C.; Yu, J. M.; Chan, C. Y.; Wong, P.K. Effective Photocatalytic Disinfection of E. Coli K-12 Using AgBr-Ag-Bi_2WO_6 Nanojunction System Irradiated by Visible Light: The Role of Diffusing Hydroxyl Radicals. *Environ. Sci. Technol.* **2010**, *44*, 1392−1398.

(9) McCullagh, C.; Skillen, N.; Adams, M.; Robertson, P. K. J. Photocatalytic Reactors for Environmental Remediation: A Review. *J. Chem. Technol. Biotechnol.* **2011**, *86*, 1002−1017.

(10) Li, K.; He, Y.; Yu, L.; Xu; Wang, Y. L.; Jia, J. P. Degradation of Rhodamine B Using An Unconventional Graded Photoelectrode with Wedge Structure. *Environ. Sci. Technol.* **2011**, *45*, 7401−7407.

(11) Mohseni, M. Gas Phase Trichloroethylene (TCE) Photo-oxidation and Byproduct Formation: Photolysis vs. Titania/Silica Based Photocatalysis. *Chemosphere* **2005**, *59*, 335−342.

(12) Vincent, G.; Marquaire, P. M.; Zahraa, O. Abatement of Volatile Organic Compounds Using An Annular Photocatalytic Reactor: Study of Gaseous Acetone. *J. Photochem. Photobiol., A* **2008**, *197*, 177−189.

(13) Richter, O.; Hoffmann, H.; Kraushaar-Czarnetzki, B. Effect of the Rotor Shape on the Mixing Characteristics of A Continuous Flow Taylor-vortex Reactor. *Chem. Eng. Sci.* **2008**, *63*, 3504−3513.

(14) Kuo, H. P.; Wu, C. T.; Hsu, R. C. Continuous Reduction of Toluene Vapours from the Contaminated Gas Stream in A Fluidised Bed Photoreactor. *Powder Technol.* **2009**, *195*, 50−56.

(15) Zhang, Z.; Anderson, W. A.; Moo-Young, M. Experimental Analysis of A Corrugated Plate Photocatalytic Reactor. *Chem. Eng. J.* **2004**, *99*, 145−152.

(16) Pinho, L. X.; Azevedo, J.; Miranda, S. M.; Angelo, J.; Mendes, A.; Vilar, V. J. P.; Vasconcelos, V.; Boaventura, R. A. R. Oxidation of Microcystin-LR and Cylindrospermopsin by Heterogeneous Photocatalysis Using A Tubular Photoreactor Packed with Different TiO_2 Coated Supports. *Chem. Eng. J.* **2015**, *266*, 100−111.

(17) Buriak, J. M.; Kamat, P. V.; Schanze, K. S. Best Practices for Reporting on Heterogeneous Photocatalysis. *ACS Appl. Mater. Interfaces* **2014**, *6*, 11815−11816.

(18) Hoffmann, M. R.; Martin, S. T.; Choi, W. Y.; Bahnemann, D. W. Environmental Applications of Semiconductor Photocatalysis. *Chem. Rev.* **1995**, *95*, 69−96.

(19) Serpone, N.; Salinaro, A. Terminology, Relative Photonic Efficiencies and Quantum Yields in Heterogeneous Photocatalysis. Part I: Suggested Protocol (Technical Report). *Pure Appl. Chem.* **1999**, *71*, 303−320.

(20) Cheng, H.; Huang, B.; Wang, P.; Wang, Z.; Lou, Z.; Wang, J.; Qin, X.; Zhang, X.; Dai, Y. In Situ Ion Exchange Synthesis of the Novel Ag/AgBr/BiOBr Hybrid with Highly Efficient Decontamination of Pollutants. *Chem. Commun.* **2011**, *47*, 7054−7056.

(21) Schnippering, M.; Carrara, M.; Foelske, A.; Kotz, R.; Fermin, D. J. Electronic Properties of Ag Nanoparticle Arrays. A Kelvin Probe and High Resolution XPS Study. *Phys. Chem. Chem. Phys.* **2007**, *9*, 725−730.

DOI: 10.1021/acsami.5b05184
ACS Appl. Mater. Interfaces 2015, 7, 20076−20082

(22) Banerjee, M.; Sachdev, P.; Mukherjee, G. S. Preparation of PVA/Co/Ag Film and Evaluation of Its Magnetic and Microstructural Properties. *J. Appl. Phys.* **2012**, *111*, 094302.
(23) Jasso-Salcedo, A. B.; Palestino, G.; Escobar-Barrios, V. A. Effect of Ag, pH, and Time on the Preparation of Ag-Functionalized Zinc Oxide Nanoagglomerates as Photocatalysts. *J. Catal.* **2014**, *318*, 170−178.
(24) Ingram, D. B.; Linic, S. Water Splitting on Composite Plasmonic-Metal/Semiconductor Photoelectrodes: Evidence for Selective Plasmon-Induced Formation of Charge Carriers near the Semiconductor Surface. *J. Am. Chem. Soc.* **2011**, *133*, 5202−5205.
(25) Mohapatra, L.; Parida, K.; Satpathy, M. Molybdate/Tungstate Intercalated Oxo-Bridged Zn/Y LDH for Solar Light Induced Photodegradation of Organic Pollutants. *J. Phys. Chem. C* **2012**, *116*, 13063−13070.
(26) Linic, S.; Christopher, P.; Ingram, D. B. Plasmonic-Metal Nanostructures for Efficient Conversion of Solar to Chemical Energy. *Nat. Mater.* **2011**, *10*, 911−921.
(27) Gonell, F.; Haro, M.; Sanchez, R. S.; Negro, P.; Mora-Sero, I.; Bisquert, J.; Julian-Lopez, B.; Gimenez, S. Photon Up-Conversion with Lanthanide-Doped Oxide Particles for Solar H_2 Generation. *J. Phys. Chem. C* **2014**, *118*, 11279−11284.
(28) Hu, X. X.; Hu, C.; Peng, T. W.; Zhou, X. F.; Qu, J. H. Plasmon-Induced Inactivation of Enteric Pathogenic Microorganisms with Ag-AgI/Al_2O_3 under Visible-Light Irradiation. *Environ. Sci. Technol.* **2010**, *44*, 7058−7062.
(29) Hirakawa, T.; Kamat, P. V. Photoinduced Electron Storage and Surface Plasmon Modulation in Ag@TiO_2 Clusters. *Langmuir* **2004**, *20*, 5645−5647.
(30) Park, J. Y.; Baker, L. R.; Somorjai, G. A. Role of Hot Electrons and Metal-Oxide Interfaces in Surface Chemistry and Catalytic Reactions. *Chem. Rev.* **2015**, *115*, 2781−2817.
(31) Lee, H.; Nedrygailov, I. I.; Lee, C.; Somorjai, G. A.; Park, J. Y. Chemical Reaction-induced Hot Electron Flows on Pt Colloid Nanoparticles under Hydrogen Oxidation: Impact of Nanoparticle Size. *Angew. Chem., Int. Ed.* **2015**, *54*, 2340−2344.
(32) Lee, Y. K.; Lee, J.; Lee, H.; Lee, J. Y.; Park, J. Y. Probing Polarization Modes of Ag Nanowires with Hot Electron Detection on Au/TiO_2 Nanodiodes. *Appl. Phys. Lett.* **2013**, *102*, 123112.
(33) Hu, C.; Peng, T. W.; Hu, X. X.; Nie, Y. L.; Zhou, X. F.; Qu, J. H.; He, H. Plasmon-Induced Photodegradation of Toxic Pollutants with Ag-AgI/Al_2O_3 under Visible-Light Irradiation. *J. Am. Chem. Soc.* **2010**, *132*, 857−862.

DOI: 10.1021/acsami.5b05184
ACS Appl. Mater. Interfaces 2015, 7, 20076−20082